Numerical Simulation of Stress Wave Propagation in the Three-Layer Medium Structure of Standing Trees

Yingchun Gong, a,b Jialei Qu, Haiqing Ren, a,b* Shubing Chen, and Fenglu Liu d,*

Based on the theory of stress wave propagation in solid media, this paper conceptualizes standing trees as a three-layer composite material comprising the pith, heartwood, and sapwood. Assuming that standing trees exhibit orthotropic anisotropy, the propagation process of stress waves within the trees is simulated and analyzed using the finite element simulation software. The paper investigates the effects of diameter at breast height (DBH) of 40-year-old standing larch trees and the proportional composition of pith, heartwood, and sapwood on the propagation of stress waves. The results reveal that, despite variations in DBH and the relative proportions of the three components, the overall propagation patterns of stress waves remain largely consistent across models. Initially, stress waves propagate in the form of an inclined curved surface. As the propagation distance increases, the inclination of the wavefront gradually decreases, eventually approaching a plane perpendicular to the longitudinal axis of the standing tree. When the DBH increases from 30 cm to 50 cm, the stress wave velocity rises significantly from 3,450 m/s to 3,620 m/s. Additionally, as the proportion of sapwood increases, the velocity increases from 3,529 m/s to 3,916 m/s. A strong correlation is observed between wave velocity and the compositional ratio of the three components, with a correlation coefficient (R2) of 0.98.

DOI: 10.15376/biores.20.4.8456-8472

Keywords: Standing tree; Stress wave propagation; Numerical simulation; Three-layer medium structure

Contact information: a: Research Institute of Wood Industry, Chinese Academy of Forestry, Beijing 100091, China; b: Collaborative Innovation Center for Efficient Processing and Utilization of Forest Products, Nanjing 210037, Jiangsu, China; c: China Academy of Building Research, Beijing 100032, China; d: College of Mechanical and Electrical Engineering, Fujian Agriculture and Forestry University, Fuzhou 350001, Fujian, China; *Corresponding author: renhq@caf.ac.cn, liufenglu39@fafu.edu.cn

INTRODUCTION

The application of stress wave nondestructive testing technology to assess the mechanical properties of standing trees *in situ* – thereby enabling the prediction and evaluation of the mechanical properties and quality grade of corresponding logs – has emerged as a research focus among forestry professionals and researchers both in China and abroad (Xu and Wang 2014; Liu *et al.* 2015). Due to the differences in the propagation process and mode of stress waves between standing trees and logs, the underlying propagation mechanisms or theoretical frameworks connecting the two remain insufficiently understood, making it infeasible to accurately predict or assess the quality grade of logs solely based on the mechanical properties of standing trees. To date, a number of scholars have investigated the theory of stress wave propagation in logs, contributing to a relatively deep understanding of the propagation theory of stress wave propagation in logs (including wave propagation process and modes), and yielding significant research outcomes (Martin and Berger 2003; Xu *et al.* 2014).

Based on the simplification of log specimens as uniform elastic rods with constant cross-sections, researchers have established a theoretical framework for stress wave propagation in logs. They derived the wave equations governing axial stress wave propagation and obtained analytical expressions for displacement, velocity, stress, and strain in the axial, radial, and tangential directions of the logs (Martin and Berger 2001; Yang and Wang 2005). Additionally, drawing on the general theory of stress wave propagation in solid media, further studies analyzed the differential equations governing wave propagation in logs and proposed models formulated in cylindrical polar coordinates (Martin 2004; Feng and Li 2009). Building on this, stress wave technology has been employed to investigate propagation patterns in logs, and a corresponding stress wave velocity model for logs has been established (Wang *et al.* 2016).

In contrast, research on the propagation mechanisms of stress waves in standing trees remains relatively limited. Finite element numerical simulations have been conducted to explore stress wave propagation in two-layer standing tree models composed of heartwood and sapwood (Sun 2014; Liu *et al.* 2020). These studies also analyzed the effects of diameter at breast height (DBH) and heartwood ratio on wave propagation. Furthermore, a wave velocity conversion model between standing trees and logs was developed, and its validity and reliability were confirmed through experimental verification (Liu *et al.* 2016; Liu *et al.* 2017).

Current research on the propagation modes and patterns of stress waves is based on a two-layer model of standing trees; the findings were derived under the model assumption that the standing tree consists solely of heartwood and sapwood (Zhang *et al.* 2010; Liu 2019). However, standing trees typically comprise the pith, heartwood, sapwood, and bark. As such, the two-layer model of standing trees obviously cannot fully reflect the actual structure of standing trees. To develop a model that more accurately represents the true structure of standing trees, this paper builds upon previous research by using the finite element simulation software COMSOL Multiphysics to construct a three-layer standing tree model that includes the pith, heartwood, and sapwood. Given that the mechanical properties of bark are too weak to be effectively modeled, the bark is excluded from the simulation. Through numerical simulation, the paper explores the propagation modes and patterns of stress waves in the three-layer model and analyzes how variations in the proportional composition of pith, heartwood, and sapwood impact stress wave propagation.

EXPERIMENTAL

Geometric Modeling of the Standing Tree

Wood consists of multiple anatomical components, including the pith, heartwood, sapwood, and bark. As a naturally and highly anisotropic material, the mechanical properties of standing trees vary significantly among the pith, heartwood, and sapwood. To investigate the impact of varying proportions of these components on stress wave propagation, certain reasonable simplifications of standing trees are necessary (Liu *et al.* 2019):

- 1) The standing tree is assumed to be an orthotropic material;
- 2) It is assumed that the standing tree can be accurately modeled as a three-layer structure composed of pith, heartwood, and sapwood, with each layer exhibiting orthotropic properties.

3) For a 40-year-old *Larix gmelinii* var. *principis-rupprechtii* (North China larch) standing tree, the DBH typically ranges from 15 to 40 cm, with an average taper of approximately 1 to 3 cm/m. The ratio of pith, heartwood, and sapwood content generally falls within the range of 1:3:6 to 1:1:8 (Zhu 2018). In light of these structural characteristics, the standing tree is modeled as a tapered cylindrical body with a length *L* of 200 cm and a taper of 1.5 cm/m. The large-end diameter D is set to 35 cm, while the small-end diameter *d* is set to 32 cm. To analyze the impact of varying pith, heartwood, and sapwood proportions on stress wave propagation of standing trees, five different component ratio scenarios (denoted as *k*) were selected: 1:1:8, 1:1.5:7.5, 1:2:7, 1:2.5:6.5, and 1:3:6. The geometric parameters corresponding to each of the five standing tree models are detailed in Table 1.

Table 1. Three-Dimensional Geometric Dimensions of Five Standing Tree Models with Different Ratios of Pith, Heartwood, and Sapwood

Variables	Model 1	Model 2	Model 3	Model 4	Model 5
L (cm)	200	200	200	200	200
k	1:3:6	1:2.5:6.5	1:2:7	1:1.5:7.5	1:1:8
R₁ (cm)	10.5	11.375	12.25	13.125	14
R ₂ (cm)	5.25	4.375	3.5	2.625	1.75
R₃ (cm)	1.75	1.75	1.75	1.75	1.75
r₁ (cm)	9.6	10.4	11.2	12	12.8
r ₂ (cm)	4.8	4	3.2	2.4	1.6
<i>r</i> ₃ (cm)	1.6	1.6	1.6	1.6	1.6

Note: L denotes the model length; k represents the ratio of pith, heartwood, and sapwood; R_1 , R_2 , and R_3 refer to the radii at the larger end of the sapwood, heartwood, and pith layers, respectively; while r_1 , r_2 , and r_3 denote the radii at the smaller end of the same layers, respectively.

Using Model 1 as an example, the three-dimensional geometric model of the standing tree constructed in the software is shown in Fig. 1.



Fig. 1. Three-dimensional geometric model of standing trees in model 1. (1) Pith layer; (2) heartwood layer; (3) sapwood layer. All coordinate axes are in cm.

To investigate the impact of DBH on stress wave propagation, five groups of standing tree models with DBH values of 10, 30, 50, 70, and 90 cm were established. The specific dimensional parameters of these models are shown in Table 2.

Table 2. Dimension Parameters of the Geometric Models for Standing Trees with Different DBH Values

	Model 1	Model 2	Model 3	Model 4	Model 5
L (cm)	200	200	200	200	200
D_1 (cm)	10	30	50	70	90
d₁ (cm)	7	27	47	67	87
D_2 (cm)	4	12	20	28	36
d ₂ (cm)	2.8	10.8	18.8	26.8	34.8
D_3 (cm)	1	3	5	7	9
d ₃ (cm)	0.7	2.7	4.7	6.7	8.7

Note: D_1 , D_2 , and D_3 represent the diameters at the large end of the sapwood, heartwood, and pith, respectively, while d_1 , d_2 , and d_3 represent the corresponding diameters at the small end.

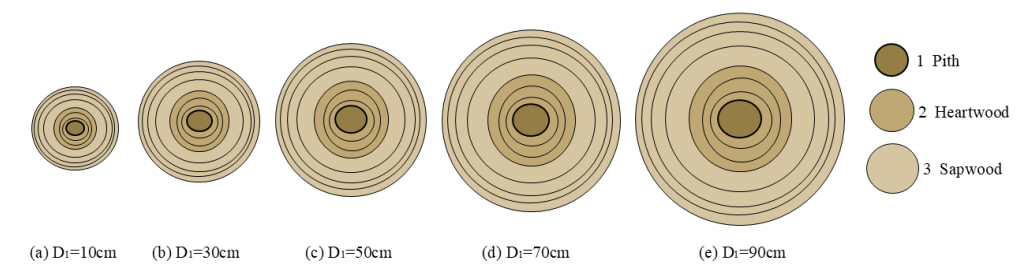


Fig. 2. Diagram of the large end of standing larch tree models with different DBH values

Material Properties

The material property parameters for the pith, heartwood, and sapwood layers in this study were obtained from prior mechanical experiments on larch standing trees. These experiments measured all 12 elastic constants at four different sampling positions (Liu *et al.* 2015). The specific parameters are presented in Tables 3, 4, and 5. In these tables, E_L denotes the longitudinal elastic modulus, E_T the tangential elastic modulus, and E_R the radial elastic modulus. G_{RT} , G_{LR} , and G_{LT} represent the shear moduli in the R–T, L–R, and L–T planes, respectively. v_{RT} , v_{LR} , and v_{LT} refer to Poisson's ratios in the R–T, L–R, and L–T directions, respectively. The densities of the pith, heartwood, and sapwood layers in the standing tree model are 350 kg/m³, 500 kg/m³, and 750 kg/m³, respectively.

Table 3. Elastic Constant and Density Values of Pith

Elastic Modulus (MPa)		Shear Mod	Shear Modulus (MPa)		s Ratio	Density (kg/m³)
E∟	5016	G RT	326	V LT	0.15	
E ⊤	339	G_{LR}	538	V LR	0.13	350
E R	628	G_{LT}	403	V RT	0.74	

Table 4. Elastic Constant and Density Values of Heartwood

Elastic Modulus (MPa)		Shear Mod	near Modulus (MPa)		s Ratio	Density (kg/m³)
<i>E</i> ∟	7629	G_{RT}	450	V LT	0.30	
E ⊤	362	G_{LR}	428	V LR	0.22	500
E R	773	G_{LT}	393	V RT	0.77	

Table 5. Elastic Constant and Density Values of Sapwood

Elastic Modulus (MPa)		Shear Modulus (MPa)		Poisson's Ratio		Density (kg/m³)
E_{L}	10137	G_{RT}	556	V_{LT}	0.36	
E ⊤	282	G_{LR}	430	V LR	0.26	750
E R	342	G_{LT}	446	V RT	0.81	

External Load Setting

Referring to the *in situ* stress wave testing method for standing trees (Zhang *et al.* 2010), the external impact load applied in the numerical simulation in this study is expressed as follows,

$$F(t) = \begin{cases} A\sin(2\pi f t) & t < (1/2f) \\ 0 & t \ge (1/2f) \end{cases}$$
(1)

where A denotes the amplitude and f represents the frequency of the external impact load. Based on actual measurements of the external impact load from the hammer, as shown in Fig. 3, the amplitude of the actual external impact load is approximately 200 N, with a duration of about 200 ms, corresponding to a frequency of approximately 2.5 kHz.

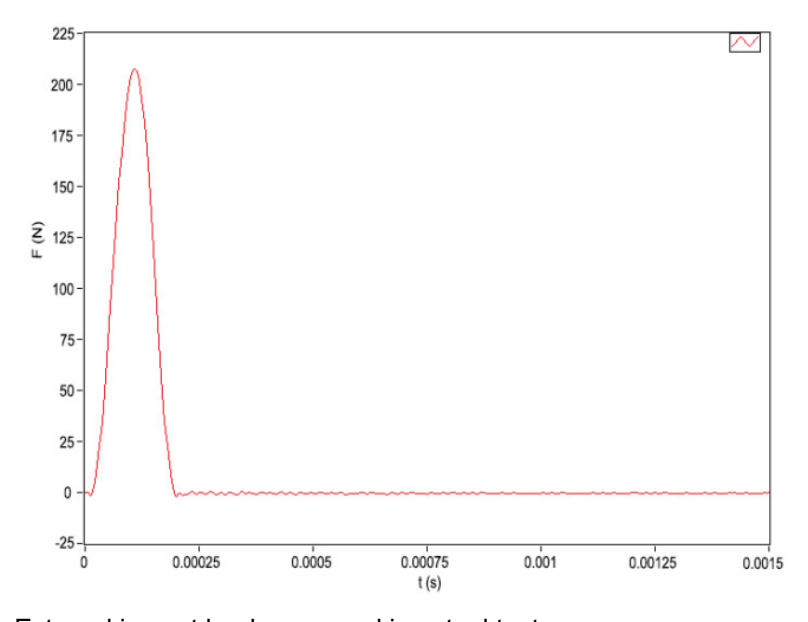


Fig. 3. External impact load measured in actual tests

According to the *in situ* stress wave testing method for standing trees, the stress waves within the tree are typically generated by an oblique impact. The external impact load F(t) was decomposed into two components along the Y and Z axes: $F_y(t)$ and $F_z(t)$, each with an amplitude of 141.4 N and an impact frequency of f = 2.5 kHz. The function of each external impact load is shown in Fig. 4.

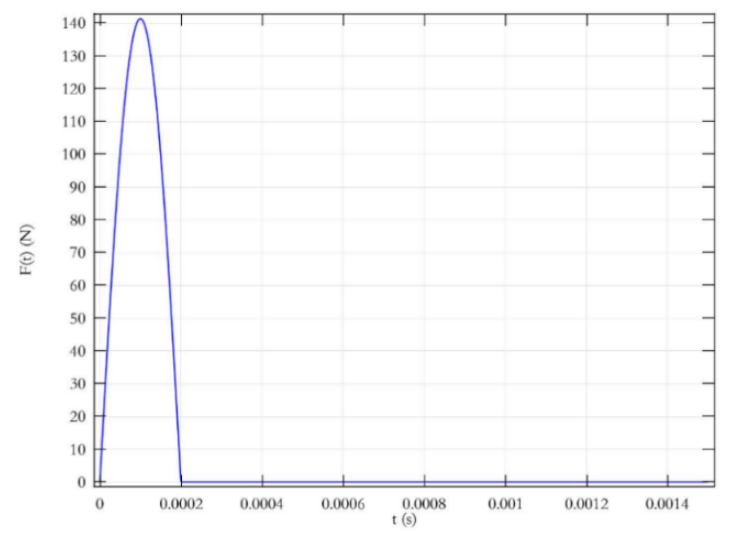


Fig. 4. Function of half-sine pulse

Initial and Boundary Conditions

Initial conditions

The initial conditions include both the initial displacement (Eq. 2) and initial velocity (Eq. 3), which were calculated as follows.

$$u_i = 0 \quad (i = x, y, z) \tag{2}$$

$$\frac{\partial u_i}{\partial t} = 0 \quad (i = x, y, z) \tag{3}$$

where u_i is the displacement of a particle, t is the time, and x, y, and z are the spatial coordinates of the particle.

Boundary conditions

In the numerical simulation, the lateral surface of the three-dimensional standing tree model is subjected to a free boundary condition (Eq. 4), while the remote end face of the model is assigned a low-reflecting boundary condition (Eq. 5), as follows,

$$\left. \frac{\partial u}{\partial l} \right|_{(x^2 + y^2 = r_2^2, 0 \le z \le 500)} = 0 \tag{4}$$

$$\sigma \cdot n = -\rho \cdot C_p(\frac{\partial u}{\partial t} \cdot n) \cdot n - \rho \cdot C_s(\frac{\partial u}{\partial t} \cdot t) \cdot t \tag{5}$$

where l is the unit normal vector, r_2 is the radius at the large end of the standing tree model, σ is the stress acting on internal particles, n and t represent the unit normal and unit tangential vectors, respectively, C_p is the longitudinal wave velocity, C_s is the shear wave velocity, and ρ is the density of the medium.

Mesh Generation and Solver Settings

Taking Model 1 as an example, the three-dimensional model was meshed using the sweep method. The maximum element size was 11 cm, the minimum element size to 0.8 cm, and 30 distribution elements were used. After meshing, the total number of elements in the full three-dimensional model was 7,869. Figure 5 presents the meshing result of the standing tree model (Model 1).

The solver step sizes for the three-dimensional model were configured as follows. For transient analysis, a generalized- α free time-stepping method was employed, with both the initial and maximum time steps set to the system default values. The computation time step was set to 4×10^{-6} s, and the output time step for solution results was set to 5×10^{-7} s.

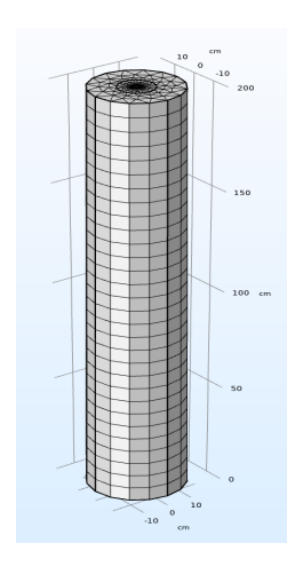


Fig. 5. Diagram of three-dimensional meshing of standing tree model (Model 1)

RESULTS AND DISCUSSION

Three-Dimensional Displacement Isosurface Diagrams

Standing tree models with different proportions of pith, heartwood, and sapwood

From the results of the three-dimensional numerical simulations, displacement isosurface diagrams were generated at five selected time points: t=100, 200, 300, 400, and 500 μ s, depicting the propagation of stress waves in standing tree models with varying proportions of pith, heartwood, and sapwood. Using Model 1 as an example, the simulation results are presented in Fig. 6. At each time point, the frontmost isosurface of the three-dimensional displacement isosurface diagrams represents the wavefront of the stress wave at that specific time. For all standing tree models with different proportions of pith, heartwood, and sapwood, the point of impact generating the stress wave is located at the lower-left corner of the model.

The stress wave in the three-layer standing tree models—with varying proportions of pith, heartwood, and sapwood—initially propagates as an inclined curved surface, exhibiting a steep inclination and bending toward the input side of the impact load. As the propagation time increases and the stress wave travels farther, the curved surface of wavefront elongates, while its inclination gradually decreases. Eventually, the wavefront shortens and transitions into a planar shape, becoming more perpendicular to the lengthwise direction of the standing tree. This indicates that the stress wave propagation in the standing tree evolves from a three-dimensional expanding wave into a one-dimensional planar wave.

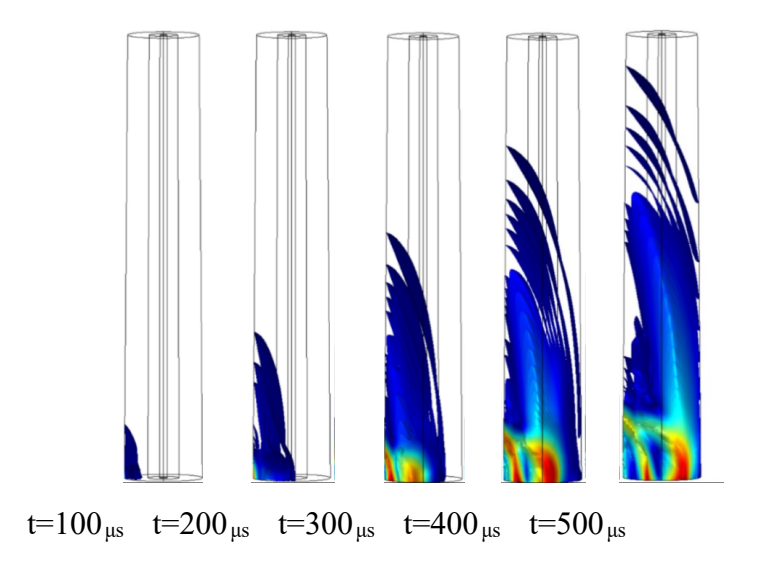


Fig. 6. Three-dimensional displacement isosurface of stress wave propagation in standing tree models with different proportions of pith, heartwood, and sapwood (Model 1)

Standing tree models with different DBH values

For standing tree models with different DBH values, displacement isosurface diagrams at selected time points (t = 100, 200, 300, 400, and $500^{\mu s}$) were generated from the three-dimensional numerical simulation results to depict the propagation of stress waves. Using Model 3 as an example, the simulation results are illustrated in Fig. 7. At each time point, the frontmost isosurface in the three-dimensional displacement isosurface diagrams represents the wavefront of the stress wave at that specific time point. It is important to note that for all standing tree models with different DBH values, the point of impact generating the stress wave is located at the lower-right corner of the model.

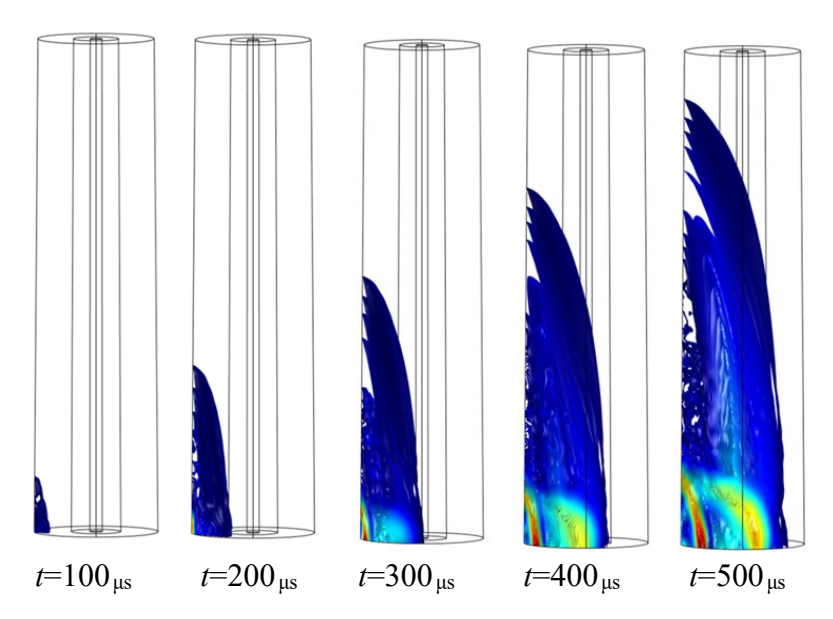


Fig. 7. Three-dimensional displacement isosurface of stress wave propagation in standing tree models with different DBH values (Model 3)

The propagation mode and pattern of stress waves in standing tree models with different DBH values are essentially the same as those observed in models with varying proportions of pith, heartwood, and sapwood. Initially, the stress waves propagate as an inclined curved surface, exhibiting a steep inclination and bending toward the input side of the impact load. As the propagation time increases and the stress wave propagates farther, the curved surface of wavefront elongates, while its inclination gradually decreases. Eventually, the wavefront shortens and transitions into a planar shape, becoming more perpendicular to the lengthwise direction of the standing tree.

Three-Dimensional Wavefront Diagrams Of Stress Wave Propagation

Standing tree models with different proportions of pith, heartwood, and sapwood

To illustrate the propagation process of the stress wavefront throughout the standing tree, and to examine whether the propagation process is affected by the proportions of pith, heartwood, and sapwood, the frontmost isosurfaces were extracted from the displacement isosurface diagrams at multiple time points (t = 100, 150, 200, 250, 300, 350, 400, 450 and 500 μ s). Using software post-processing techniques, the three-dimensional wavefront diagrams of stress wave propagation were generated for the five standing tree models with different proportions of pith, heartwood, and sapwood. These results are shown in Fig. 8.

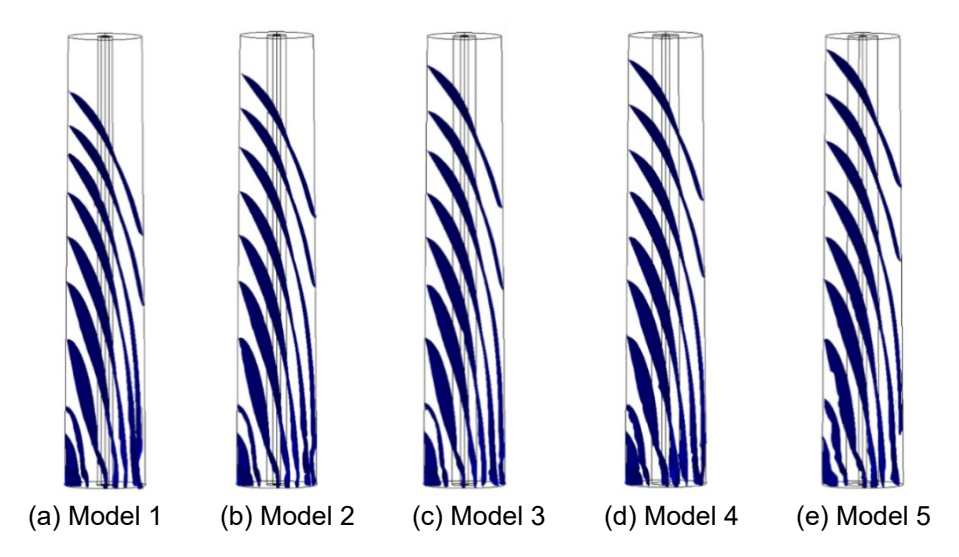


Fig. 8. Three-dimensional wavefront diagrams of stress wave propagation in standing tree models with different proportions of pith, heartwood, and sapwood

The propagation mode and pattern of stress waves in standing tree models with different proportions of pith, heartwood, and sapwood are generally identical. Initially, the stress waves propagate as an inclined curved surface, exhibiting a steep inclination and bending toward the input side of the impact load. As the propagation time increases, the curved surface of wavefront elongates, while its inclination gradually decreases. Eventually, the wavefront shortens and transitions into a planar shape, becoming more perpendicular to the lengthwise direction of the standing tree. This indicates that changes in the proportions of pith, heartwood, and sapwood do not affect the stress wave propagation mode or the shape of the wavefronts in the standing tree model. Furthermore, Figure 8 reveals that as the proportion of heartwood decreases and the proportion of sapwood increases, the propagation distance of the stress wavefront increases accordingly.

At the same simulation time point of 500 µs, the wavefront in Model 5 (with a ratio of pith, heartwood, and sapwood set at 1:1:8) travels the farthest, whereas in Model 1 (with a ratio of 1:3:6) it travels the shortest. This trend remains consistent across other time points: As the heartwood proportion decreases and the sapwood proportion increases, the propagation distance of the stress wave in standing trees increases. Therefore, while changes in the proportions of pith, heartwood, and sapwood do not affect the mode of wave propagation or the shape of the wavefront, they do affect the stress wave propagation distance. This further indicates that stress wave propagation velocity in standing trees may be affected by the relative proportions of the three components, and a certain correlation may exist between them. These simulation results are largely consistent with the findings of Liu *et al.* (2020), who investigated stress wave propagation in a two-layer standing tree model (composed only of heartwood and sapwood).

Standing Tree Models with Different DBH Values

To examine whether DBH affects the stress wave propagation process in standing tree models, the frontmost isosurfaces were extracted from the three-dimensional displacement isosurface diagrams at multiple simulation time points (t = 100, 150, 200, 250, 300, 350, 400, 450,or 500 μ s). Through software post-processing techniques, the three-dimensional wavefront diagrams of stress wave propagation were generated for five standing tree models with different DBH values. The results are shown in Fig. 9.

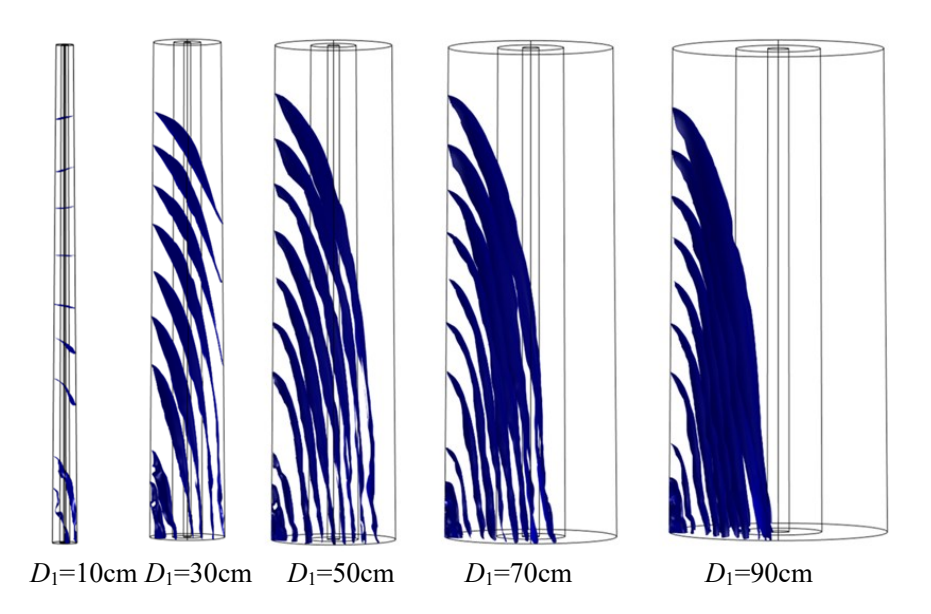


Fig. 9. Three-dimensional wavefront diagrams of stress wave propagation in standing tree models with different DBH values

When the DBH of the standing tree is 10 cm, the isosurface diagram has already advanced close to the top end of the model after 500 µs of stress wave propagation. The shape of the wavefront has largely transitioned into a one-dimensional planar surface parallel to the top-end and bottom-end faces. In contrast, as the DBH increases, the stress wavefront remains inclined at the same propagation time, with a larger DBH resulting in a greater inclination, forming an elongated, tilted curved surface. Figure 9 reveals clear visual differences in stress wave propagation diagrams across standing trees with different DBH values. As the DBH increases, more time is required for the stress wave to evolve

into a stable one-dimensional wavefront. For instance, in the model with a 10 cm DBH, the wavefront has already transitioned from a three-dimensional expanding wave to a twodimensional horizontal planar wavefront by propagation of approximately 250 to 300 µs. However, in models with a DBH greater than 30 cm, the wavefront remains in a threedimensional expanding state even after propagation of 500 us. Nevertheless, with continued propagation, the inclination of the wavefront gradually decreases, with a slow transition toward a one-dimensional planar wavefront. These observations suggest that the propagation shape of stress waves in standing trees is affected by DBH. When the DBH is relatively small, the wavefront within the tree quickly transitions from a three-dimensional expanding wave to a one-dimensional planar wave. As the DBH increases, the time required for this transition becomes longer. Additionally, Fig. 9 indicates that DBH also affects the stress wave propagation velocity. At a propagation time of 500 μs, the wavefront in the 30 cm DBH model has advanced farther than that in the 10 cm DBH model. In the 50 cm DBH model, the wavefront has propagated even farther than in the previous two models. However, for the 70 cm and 90 cm DBH models, the wavefront displacement distance shows no significant difference compared to the 50 cm model within the same time frame.

Impact of the Proportions of Pith, Heartwood, and Sapwood on Stress Wave Velocity

As observed from the three-dimensional wavefront diagrams of stress wave propagation (Fig. 8), the proportions of pith, heartwood, and sapwood in standing trees influences the propagation velocity of stress waves. To further analyze the relationship between stress wave propagation velocity and the relative proportions of these three components, numerical simulations were conducted to calculate the propagation velocities under different structural ratios, followed by a linear correlation analysis. The results are presented in Table 6 and Fig. 10.

Table 6. Propagation Velocity of Stress Wave in Five Standing Tree Models

Model (ratios of pith, heartwood, and sapwood)	Wave Velocity (m/s)
Model 5 (1:1:8)	3916
Model 4 (1:1.5:7.5)	3812
Model 3 (1:2:7)	3750
Model 2 (1:2.5:6.5)	3667
Model 1 (1:3:6)	3529

The proportions of pith, heartwood, and sapwood significantly influence the stress wave propagation velocity in standing trees. A strong correlation ($R^2 = 0.98$) is observed between stress wave velocity and the relative proportions of these three components. As the proportion of sapwood increases within the model, the stress wave propagation velocity also increases. This trend may be attributed to the substantially higher longitudinal elastic modulus of sapwood compared to that of the pith and heartwood. As the sapwood proportion increases, the impact of its longitudinal elastic modulus on the stress wave propagation velocity becomes more pronounced, eventually dominating the stress wave propagation velocity. Given that stress waves propagate most rapidly in the longitudinal direction, this results in an overall increase in propagation velocity.

In numerous studies on stress wave propagation, it has been observed that the wave velocity measured in standing trees is 7 to 36% higher than that measured in logs. This

discrepancy has been attributed to the use of the time-of-flight (TOF) method for measuring the time of stress wave propagation in standing trees, which primarily captures the wave velocity within the sapwood rather than across the entire tree cross-section (Grabianowski et al. 2004; Chauhan and Walker 2006; Mora et al. 2009). However, the results presented in Table 6 and Fig. 10 clearly indicate that the proportions of pith, heartwood, and sapwood significantly affect wave velocity in standing trees, with velocity decreasing as the proportions of pith and heartwood increase. According to the hypothesis proposed by Mora et al. (2009), if the wave velocity measured in standing trees reflects propagation solely in the sapwood, then variations in the proportions of pith and heartwood-provided that heartwood does not account for 100%—should not affect the measured wave speed. Yet, the numerical simulation results reveal that when the combined proportion of pith and heartwood increases from 20% to 40%, the corresponding stress wave velocity decreases from approximately 3,916 m/s to 3,529 m/s—a reduction of about 9.88%. This demonstrates the stress wave velocity reflects propagation across the entire standing tree model, not just within the sapwood. It further implies that stress wave propagation in standing trees is affected collectively by the pith, heartwood, and sapwood. Therefore, interpreting the higher wave velocity in standing trees as solely the result of sapwooddominated propagation—as suggested by the TOF hypothesis—may be unreasonable. The findings of this paper provide additional evidence that both experimentally measured and numerically simulated stress wave velocities in standing trees reflect propagation velocity across the whole tree structure. In other words, the impact of pith and heartwood cannot be neglected. Stress wave propagation velocity in standing trees is thus determined by the combined action of pith, heartwood, and sapwood, and the stress wave propagation process is affected by the joint influence of all three components.

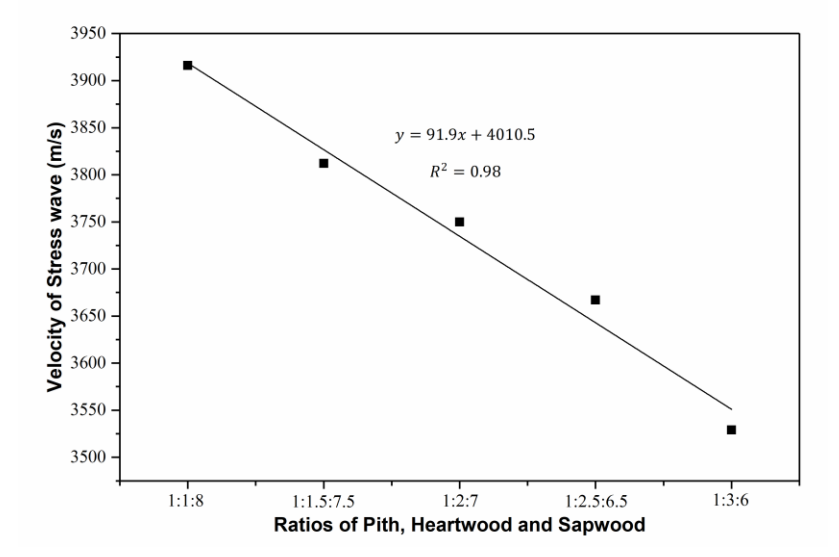


Fig. 10. Linear correlation analysis between stress wave velocity and the proportions of pith, heartwood, and sapwood

Impact of DBH Values on Stress Wave Velocity in Standing Trees

As shown in the three-dimensional wavefront diagrams of stress wave propagation (Fig. 9), the DBH of the standing tree significantly impacts the stress wave propagation velocity. To further analyze the relationship between stress wave propagation velocity and DBH, numerical simulations were conducted to calculate the propagation velocities in

standing tree models with varying DBH values. The results are presented in Table 7 and Fig. 11.

Table 7. Propagation Velocity of Stress Wave in Five Standing Tree Models with Different DBH Values

Diameter at the Large End <i>D</i> ₁ /cm of Standing Tree Model (cm)	Wave Velocity (m/s)
10	3433
30	3451
50	3620
70	3625
90	3657

As shown in Table 7 and Fig. 11, DBH significantly impacts the stress wave propagation velocity in standing trees. When the DBH is small, wave velocity changes remain minimal. In models with DBH values of 10 and 30 cm, the wave velocities are 3,433 m/s and 3,451 m/s, respectively—both slightly exceeding the theoretical velocity of a one-dimensional planar wave (3,335 m/s), which is derived from the average elastic constants and density of *Larix gmelinii* var. *principis-rupprechtii* (North China larch). In contrast, the wave velocity in the 90 cm DBH model is 3,657 m/s, lower than the theoretical velocity of a three-dimensional expanding wave (3,935 m/s). It is predicted that when the DBH falls below 10 cm, the simulated wave velocity will gradually converge to the theoretical velocity of the one-dimensional planar wave. Conversely, when DBH exceeds 90 cm, the simulated wave velocity is expected to align with the three-dimensional expanding wave. Notably, once DBH exceeds 30 cm, the stress wave velocity increases rapidly. However, after DBH exceeds 70 cm, the rate of increase begins to plateau.

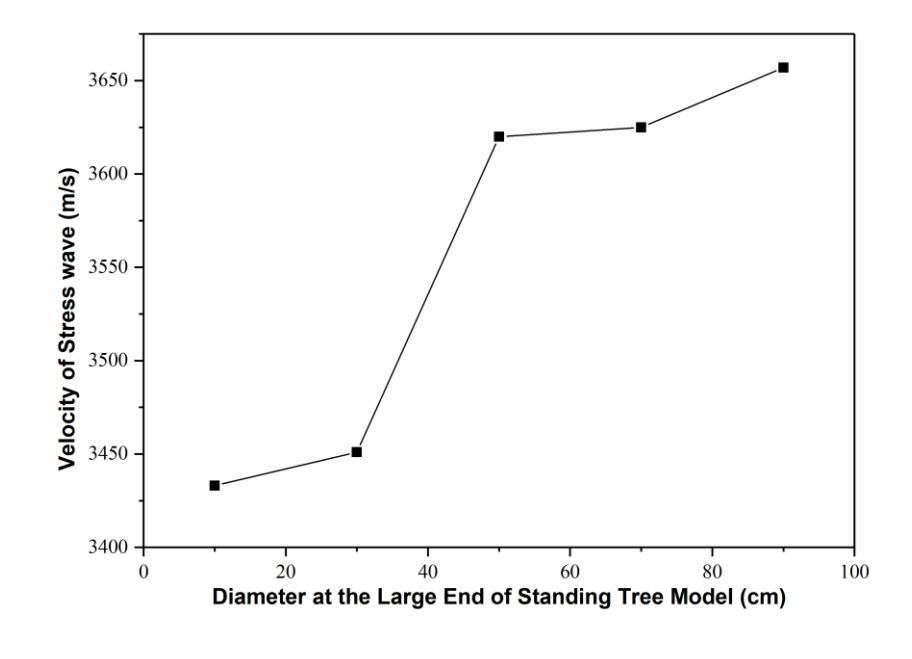


Fig. 11. Relationship between stress wave velocity and DBH of standing trees

To determine the correlation between stress wave velocity and DBH, a linear correlation analysis was conducted. The result is presented in Fig. 12, which indicates a

strong correlation (R²=0.86) between stress wave velocity and the DBH of standing trees. Stress wave velocity increases with DBH. Thus, stress wave velocity in standing trees is influenced not only by the proportions of pith, heartwood, and sapwood, but also by DBH.

Although many studies have examined the relationship between DBH and stress wave velocity, the results vary considerably, and no consistent conclusion has been reached. For example, the studied different forest stands and found almost no correlation between stress wave propagation velocity and DBH (Toulmin and Raymond 2007). Their findings are similar to other researchers (Grabianowski *et al.* 2004; Mora *et al.* 2009; Mahon *et al.* 2009). In contrast, there is a negative correlation between DBH and stress wave velocity in young plantation trees using the Fakopp device (Lasserre *et al.* 2004; Lasserre *et al.* 2005; Chauhan and Walker 2006). However, the identified a positive correlation between DBH and wave velocity and proposed a correction method based on a simple nonlinear model, using DBH as an independent variable (Wang *et al.* 2007). As shown in Fig. 11, wave velocity increases with DBH when the latter ranges from 10 cm to 90 cm, aligning with the findings of previous research (Wang *et al.* 2007). This further supports the validity of their proposed wave velocity correction model using DBH as a variable. Therefore, DBH should be considered a key variable in future models for correcting stress wave velocity in standing trees.

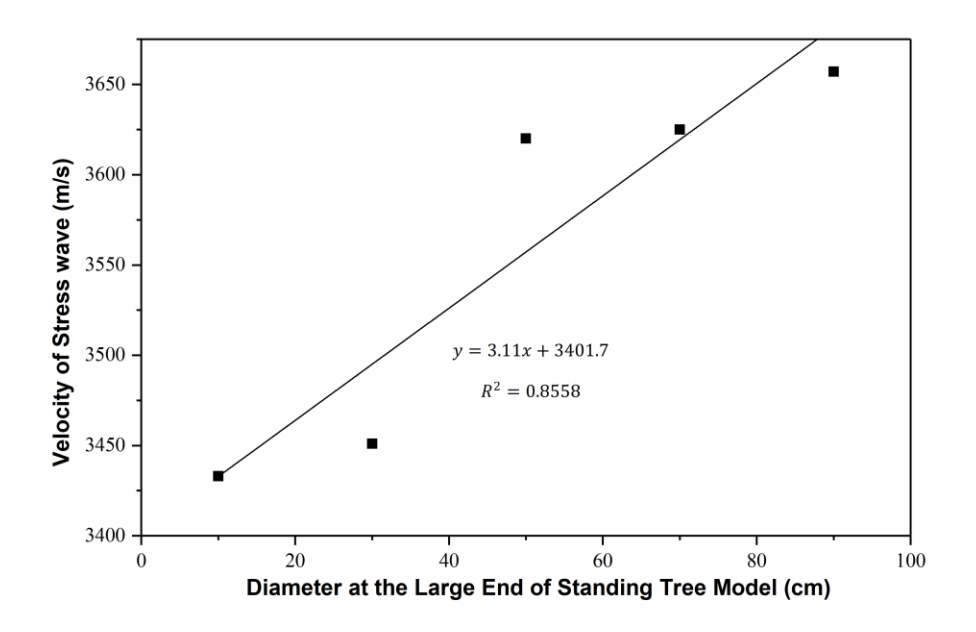


Fig. 12. Linear correlation analysis between stress wave velocity and DBH of standing trees

CONCLUSIONS

1. Variations in the proportions of pith, heartwood, and sapwood do not influence the stress wave propagation mode or the shape of the wavefront in standing tree models. The stress wave propagation mode and pattern remain generally consistent across models with different proportions of these three components. Initially, the waves propagate as an inclined curved surface, exhibiting a steep inclination and bending toward the input side of impact load. As propagation time increases, the wavefront elongates while its inclination gradually decreases. Eventually, the wavefront shortens

and transitions into a planar shape, becoming more perpendicular to the longitudinal axis of the tree.

- 2. Variations in the proportions of pith, heartwood, and sapwood influence both the propagation distance and velocity of stress waves in standing trees. As the proportion of heartwood decreases and the proportion of sapwood increases in a standing tree model, both the distance and velocity of stress wave propagation increase gradually. When the combined proportion of pith and heartwood increases from 20% to 40%, the corresponding stress wave velocity decreases from approximately 3,916 m/s to 3,529 m/s—a reduction of about 9.88%. A significant correlation is observed between stress wave velocity and the proportions of the three components (R² = 0.98).
- 3. There seems to be a significant correlation (R² = 0.86) between stress wave velocity and the DBH of standing trees. As the DBH of a standing tree model increases, stress wave velocity rises accordingly. When the DBH of a standing tree model falls below 10 cm, the wave velocity of numerical simulation gradually approaches the theoretical wave velocity of a one-dimensional planar wave. Conversely, when the DBH exceeds 90 cm, the wave velocity of numerical simulation tends toward the theoretical wave velocity of a three-dimensional expanding wave. Both DBH and the proportions of pith, heartwood, and sapwood jointly influence the mode and pattern of stress wave propagation in standing trees.

ACKNOWLEDGEMENTS

This study was carried out with the support of Scientific and Technological Innovation 2030-Major Project "Properties and Quality Evaluation of Pine Wood for Pulp and Structural Materials" (grant number 2023ZD0405905), the National Natural Science Foundation of China (No. 32301515) and Central Financial Forest and Grass Technology Promotion Demonstration Project "Promotion and demonstration of key technologies for the production of cross laminated timber from typical tree species in daxing anling region" (Daxing anling Group [2024] TG 003).

Author Contributions

Yingchun Gong: Investigation, data curation, writing-original draft, Funding acquisitio. Jialei Qu and Shubing Chen: Investigation, data curation. Haiqing Ren: data curation and review. Fenglu Liu: Conceptualization, Writing - Review, Editing. All authors have read and agreed to the published version of the manuscript.

Declaration of Competing Interest

The authors declare that they have no known competing financial interests or personal relationships that could have appeared to influence the work reported in this paper.

REFERENCES CITED

Chauhan, S. S., and Walker, J. C. F. (2006). "Variations in acoustic velocity and density with age, and their interrelationships in radiata pine," *Forest Ecology and Management* 229(3), 388-394. DOI: 10.1016/j.foreco.2006.04.019

- Feng, H., and Li, G. (2009). "Modeling and simulation of stress wave propagation for nondestructive testing of wood," *Journal of System Simulation* 21(8), 2373-2376.
- Grabianowski, M., Manley, B., and Walker, J. C. F. (2004). "Impact of stocking and exposure on outerwood acoustic properties of *Pinus radiata* in Eyrewell Forest," *New Zealand Journal of Forestry* 49(2), 13-17.
- Liu, G., Li, G., Sun, Y., and Fang, Y. (2015). "Model of stress wave propagation velocity inside trees," *Journal of Zhejiang A&F University* 32(1), 18-24. DOI: CNKI:SUN:ZJLX.0.2015-01-004
- Liu, F., Jiang, F., Zhang, J., Zhang, H., Wang, X., and Yang, Z. (2015). "Experimental study on the twelve elastic constants of green *Larix principis-rupprechtii* green wood," *Journal of Northwest Forestry University* 30(6), 227-231. DOI: 10.3969/j.issn.1001-7461.2015.06.41
- Liu, F., Jiang, F., Wang, X., Zhang, H., and Liu, X. (2016). "Stress wave propagation patterns in *Larix principis-rupprechtii* standing trees," *Journal of Nanjing Forestry University (Natural Sciences Edition)* 41(3), 133-139. DOI: 10.3969/j.issn.1000-2006.201609032
- Liu, F., Jiang, F., Wang, X., Zhang, H., and Yang, Z. (2016). "Two-dimensional simulation study of stress wave propagation in *Larix principis-rupprechtii* standing trees," *Journal of Northwest Forestry University* 31(4), 201-205. DOI: 10.3969/j.issn.1001-7461.2016.04.34
- Liu, F. (2019). Study on the Propagation Mechanism of Stress Waves in Plantation Standing Trees," Beijing Forestry University, Beijing.
- Liu, F., Zhang, H., Wang, X., Jiang, F., and Guang, C. (2020). "Numerical simulation of factors affecting stress wave propagation in *Larix principis-rupprechtii* standing trees," *Transactions of the Chinese Society for Agricultural Machinery* 51(2), 203-212. DOI: 10.6041/j.issn.1000-1298.2020.02.022
- Lasserre, J. P., Mason, E. G., and Watt, M. S. (2004). "The influence of initial stocking on corewood stiffness in a clonal experiment of 11 years-old *Pinus radiate* (D. Don)," *New Zealand Journal of Forestry* 49, 18-23.
- Lasserre, J. P., Mason, E. G., and Watt, M.S. (2005). "The effects of genotype and spacing on *Pinus radiata* [D. Don] corewood stiffness in an 11-year old experiment," *Forest Ecology and Management* 205, 375-383. DOI: 10.1016/j.foreco.2004.10.037
- Martin, P. A., and Berger, J. R. (2001). "Waves in wood: Free vibrations of a wooden pole," *Journal of the Mechanics and Physics of Solids* 49(5), 1155-1178. DOI: 10.1016/S0022-5096(00)00068-5
- Martin, P.A. and Berger, J. R. (2003). "Waves in wood: Axisymmetric guided waves along boreholes," *Chinese Journal of Mechanics.Series A* 19(1), 105-111. DOI: 10.1007/S00419-002-0268-z
- Martin, P. A. (2004). "Waves in wood: Axisymmetric waves in slender solids of revolution," *Wave Motion* 40(4), 387-398. DOI: 10.1016/j.wavemoti.2004.07.001
- Mora, C. R., Schimleck, L. R., Isik, F., Mahon, J.M., Clark, A., and Daniels, R. F. (2009). "Relationships between acoustic variables and different measures of stiffness in standing *Pinus taeda* trees," *Canadian Journal of Forest Research* 39(8), 1421-1429. DOI: 10.1139/X09-062
- Mahon, J. M., Jordan, L., Schimleck, L. R., Clark, A., and Daniels, R.F. (2009). "A comparison of sampling methods for a standing tree acoustic device," *Southern Journal of Applied Forestry* 33(2), 62-68. DOI: 10.1093/sjaf/33.2.62
- Sun, Y. (2014). "Study on the influencing factors of stress wave propagation in wood,"

- Hangzhou: Zhejiang A&F University.
- Toulmin, M. J., and Raymond, C. A. (2007). "Developing a sampling strategy for measuring acoustic velocity in standing *Pinus radiata* using the TreeTap time of flight tool," *New Zealand Journal of Forestry Science* 37(1), 96-111.
- Wang, X., Ross, R.J., and Carter, P. (2007). "Acoustic evaluation of wood quality in standing trees. Part I. acoustic wave behavior," *Wood and Fiber Science* 39(1), 28-38. DOI: 10.1007/s00468-006-0105-z
- Weng, X., Li, G., Feng, H., Du, X., and Chen, F. (2016). "Model of stress wave propagation velocity in the radial longitudinal section of trees," *Scientia Silvae Sinicae* 52(7), 104-112. DOI: 10.11707/j.1001-7488.20160713
- Xu, H., and Wang, L. (2014). "Impact of cavities on stress wave propagation path in wood," *Journal of Northeast Forestry University* 42(4), 82-84. DOI: 10.13759/j.cnki.dlxb.2014.04.018
- Xu, H., Xu, G., Wang, L., and Yang, X. (2014). "Isoline mapping of stress wave propagation time in log cross-sections and analysis of influencing factors," *Scientia Silvae Sinicae* 50(4), 95-100. DOI: 10.11707/j.1001-7488.20140414
- Yang, X., and Wang, L. (2005). "Theoretical study on stress wave propagation in logs," *Scientia Silvae Sinicae* 41(5), 132-138. DOI: 10.3321/j.issn:1001-7488.2005.05.024
- Zhang, H., Wang, X., Su, J., and Robert, R. (2010). "Experimental study on the propagation mechanism of stress waves in *Pinus resinosa* standing trees," *Journal of Beijing Forestry University* 32(2), 145-148. DOI: 10.13332/j.1000-1522.2010.02.023
- Zhu, F. (2018). Variation Pattern and Prediction model of Heartwood in Larix principisrupprechtii, Northeast Forestry University, Harbin, China.

Article submitted: April 29, 2025; Peer review completed: June 14, 2025; Revisions accepted: June 27, 2025; Published: August 5, 2025.

DOI: 10.15376/biores.20.4.8456-8472